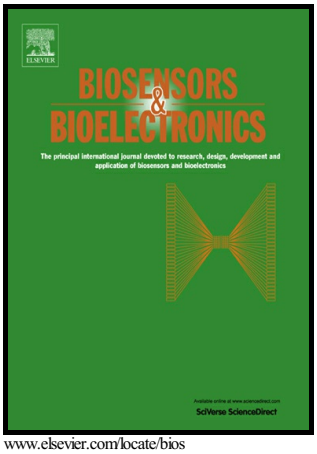

www.elsevier.com/locate/bios

A paper based graphene-nanocauliflower hybrid composite for point of care biosensing

S.L. Burrs, M. Bhargava, R. Sidhu, J. Kiernan-Lewis, C. Gomes, J.C. Claussen, E.S. McLamore

PII: S0956-5663(16)30467-5
DOI: http://dx.doi.org/10.1016/j.bios.2016.05.037
Reference: BIOS8727

To appear in: *Biosensors and Bioelectronic*

Received date: 29 March 2016
Revised date: 4 May 2016
Accepted date: 10 May 2016

Cite this article as: S.L. Burrs, M. Bhargava, R. Sidhu, J. Kiernan-Lewis, C Gomes, J.C. Claussen and E.S. McLamore, A paper based graphene nanocauliflower hybrid composite for point of care biosensing, *Biosensors an Bioelectronic,* http://dx.doi.org/10.1016/j.bios.2016.05.037

A paper based graphene-nanocauliflower hybrid composite for point of care biosensing

S.L. Burrs[1], M. Bhargava[1], R. Sidhu[2], J. Kiernan-Lewis[1], C. Gomes[2], J.C. Claussen[3], E.S. McLamore[1*]

[1]Agricultural & Biological Engineering Department, Institute of Food and Agricultural Systems, University of Florida, USA

[2]Biological & Agricultural Engineering, Texas A&M University, USA

[3]Mechanical Engineering Department, Iowa State University, USA

*Corresponding author; email: emclamor@ufl.edu

Abstract

We demonstrate the first report of graphene paper functionalized with fractal platinum nanocauliflower for use in electrochemical biosensing of small molecules (glucose) or detection of pathogenic bacteria (*Escherichia coli* O157:H7). Raman spectroscopy, scanning electron microscopy and energy dispersive spectroscopy show that graphene oxide-coated nanocellulose was partially reduced by both thermal treatment, and further reduced by chemical treatment (ascorbic acid). Fractal nanoplatinum with cauliflower-like morphology was formed on the reduced graphene oxide paper using pulsed sonoelectrodeposition, producing a conductive paper with an extremely high electroactive surface area (0.29 ± 0.13 cm^2), confirmed by cyclic voltammetry and electrochemical impedance spectroscopy. The platinum surface was functionalized with either glucose oxidase (via chitosan encapsulation) or a RNA aptamer (via covalent linking) for demonstration as a point of care biosensor. The

detection limit for both glucose (0.08 ± 0.02 µM) and *E. coli* O157:H7 (≈4 CFU mL^{-1}) were competitive with, or superior to, previously reported devices in the biosensing literature. The response time (6 sec for glucose and 12 min for *E. coli*) were also similar to silicon biochip and commercial electrode sensors. The results demonstrate that the nanocellulose-graphene-nanoplatinum material is an excellent paper-based platform for development of electrochemical biosensors targeting small molecules or whole cells for use in point of care biosensing.

Keywords

Nanocauliflower, graphene ink, nanocellulose, point of care, paper biosensor, fractal

1. Introduction

A wide variety of paper-based biosensors such as colorimetric indicators (Suaifan et al., 2013), fluorescent/chemiluminescent immunoassays (Ellerbee et al., 2009; Ge et al., 2012), microfluidic arrays (Abe et al., 2008; Chen et al., 2008; Liu and Crooks, 2011), origami immunosensors (Li et al., 2014), and electrochemical biosensors (Dungchai et al., 2009) have been developed. Development of conductive paper for electrochemical sensing based on conductive nanocarbon has been an area of extensive research for the last few decades. Conductive nanocarbon-based paper has been synthesized using fullerenes, nanotubes, and single layer nanosheets (Dikin et al., 2007; Liu, 1998; Madden et al., 2006; Park et al., 2008; Spinks et al., 2002; Zhang et al., 2004). Recently, most research in conductive paper for electrochemical biosensing has focused on use of graphene or reduced graphene oxide as the conductive backbone (Chen et al., 2008; Eda et al., 2009, 2008; Mates et al., 2015; Xu et al., 2010; Yang et al., 2013). Many groups have shown that hybrid nanostructures containing nanocarbon and nanometal are one of the most efficient platforms for electrochemical sensors and biosensors (Labroo and Cui, 2014; Xia et al., 2011). However, to date there are no examples of nanometal-graphene hybrid composites for use in paper-based biosensing.

Among the many approaches for deposition of nanometal onto conductive carbon, many groups have focused on synthesis of nanometal fractal structures with the aim of fabricating high efficiency electronic devices. For example, (Chamousis et al., 2014) recently showed that fractal silver nanostructures in organic semiconducting polymer films are more efficient than traditional “flat” photovoltaic electrodes. Wang et al

(Wang et al., 2013) developed fractal gold nanostructures for the ultra-sensitive recognition of rare cancer cells from whole blood samples. Zhou et al (Zhou et al., 2007)synthesized fractal palladium nano urchins and dendrites for use as a highly conductive platform in amperometric sensing. Nanometal structures with morphology similar to cauliflower or broccoli have been synthesized with gold (Sattayasamitsathit et al., 2013), zinc oxide (Izaki et al., 2008), iron oxide (Warren et al., 2013), and cadmium sulfide (Wilson et al., 2014). Other nanostructure morphologies such as flowers, raspberries, urchins, and confeito have also been synthesized (Liu et al., 2014; Marr et al., 2015; Ujihara and Imae, 2013; Wang et al., 2010; Wei et al., 2012). Among the various metals used to create fractal nanostructures, nanoplatinum (nPt) has properties that make it particularly useful for biosensing (it is biocompatible, easily biofunctionalized, corrosion resistant, and stable).

In this manuscript, we demonstrate the synthesis and application of platinum nanocauliflower-graphene hybrids on nanocellulose paper for use in point of care (POC) biosensing. We demonstrate use of this device in amperometric biosensing with an oxidase and a RNA aptamer for detection of glucose of *Escherichia coli* O157:H7, respectively.

2. Methods

See supplemental section for list of materials and reagents and methods for microbial cultivation.

2.1 Preparation of conductive paper

Graphene-nanocellulose paper was prepared based on modification of the recipe developed by (Marr et al., 2015). A CNC layer was first formed by vacuum filtration of a 1:4 (slurry: water) mixture through a 7.0 cm cellulose acetate filter paper (50 mL total slurry volume). The filter with CNC retentate was removed and pressed between borosilicate glass slides, and then dried at 75°C for one hour. The CNC paper was then coated with 500 µL of conductive ink, and dried in a vacuum oven at 115^{o}C for 2 hours. After this thermal reduction (referred to as thermally reduced graphene paper, or TRG), the material was immersed in 1mM ascorbic acid for one hour to chemically reduce the graphene oxide (referred to as ascorbic acid reduced graphene paper, or AARG). Finally, the samples were dried for 30 minutes at 75°C and cut into rectangular strips (1.2 cm by 0.5 cm). Platinum was electrodeposited on graphene-nanocellulose paper using pulsed sonoelectrodeposition at a frequency of 500 mHz for 180 sec at 10 V versus a bare platinum wire based on (Burrs et al., 2015; Chaturvedi et al., 2014). The conductive paper was fixed into a custom 3-D printed sample immobilization device with an open diameter of 2mm (see supplemental Figure S1).

2.2 Biofunctionalization of conductive paper

Glucose biosensors were prepared by functionalizing the nanoplatinum with glucose oxidase (GOx) entrapped in a chitosan hydrogel based on Burrs et al (Burrs et al., 2015). In summary, an aliquot (10 µL) of GOx (46mg/mL at a protein concentration of 138.4 kU/g) was mixed with 10 µL of chitosan (0.05% w/v), and vortex-agitated for 1 min. A 2 µL aliquot of enzyme-hydrogel suspension was drop-coated onto the surface of the device and dried at room temperature for 30 minutes.

Aptasensors for detecting *E. coli* by O157:H7 by were prepared by dropcasting 2μL of thiolated 64-mer RNA aptamer that is known to bind the O-antigen (K_D = 110 nM) suspended in 10 mM TRIS EDTA buffer, pH 7.4). The aptamer was allowed to adsorb for 30 minutes at room temperature.

2.3 Electrochemical Analysis

All electrochemical analysis was performed in a 3D printed sample immobilization device (see supplemental Figure S1). Cyclic voltammetry (CV) and DC potential amperometry, (DCPA) were carried out using a potentiostat (BASi, West Lafayette, USA). Electrochemical impedance spectroscopy (EIS) was conducted on a EA163 potentiostat and an eDAQ ERZ100 (eDAQ, Colorado Springs, USA).

CVs were performed in 4 mM $Fe(CN)_6$ with 100 mM KNO_3 as the electrolyte at a switching potential of 600 mV versus a Ag/AgCl reference electrode with 5 seconds quiet time at scan rates of 20, 50, 100, 150, and 200 mV s^{-1}. DCPA tests were conducted in 5 mL of PBS at a working potential of +500 mV versus a Ag/AgCl reference electrode with a sampling rate of 1 kHz. EIS was conducted in a solution of 2.5 mM $K_4Fe(CN)_6$ and 2.5 mM $K_3Fe(CN)_6$ with 1 mM KCl as the electrolyte versus a Ag/AgCl reference electrode using a bare platinum wire as the counter electrode. With a potential of 100 mV (AC) and 0.25 mV (DC) at 1 Hz were used to calculate sensitivity and LOD.

2.4 Imaging and material analysis

Raman spectra were obtained using a Horiba Aramis Raman spectrometer with a 532-nm laser source. A 100 μm confocal hole with a 1-3% transmission filter (400-3000 range) at 20 seconds per scan and 1X *ad hoc* averaging was used for all samples. Scanning electron micrographs (SEM) were captured using an FEI XL-40 FEG-SEM, with accelerating voltage of 20 kV (100kX). Electron dispersive X-ray spectroscopy (EDS) was conducted with a solid state EDAX silicon drift detector (20 kX) on a SEM 6400 for elemental analysis.

3. Results and Discussion

3.1 Material Analysis and Surface Morphology

Raman spectroscopy was used to characterize thermally reduced (TRG) and chemically reduced (AARG) nanocellulose paper (λ_x = 532 nm). Stokes and anti-stokes peaks associated with graphene are clearly visible in **Fig 1 A-C (**Raman spectra between 1000 to 3000 cm^{-1} can be seen in supplemental Figure S2). The anti-stokes shift appears in the D-band (1364.5 $\pm$ 1.4 cm^{-1}), while the stokes shift is reflected in the G-band (1593.1 $\pm$ 1.4 cm^{-1}) and the 2D-band (2718.8 $\pm$ 5.2 cm^{-1}) (Kabiri et al., 2014; Zhang et al., 2016). The D-band, G-band and 2D-band for pristine graphene (shown as a dashed line in **Fig. 1**) are located at approximately 1330 cm^{-1}, 1586 cm^{-1}, and 2690 cm^{-1}, respectively; these lines are slightly different than the graphene nanocellulose hybrid material developed here (Childres et al., 2013; Stankovich et al., 2007). The G-band is related to graphitic components, while the D-band is associated with structural defects and partially disordered structures of sp^2 domains (Kabiri et al., 2014; Stankovich et al., 2007; Zhang et al., 2016). The appearance of a distinct peak near the

D-band (**Fig 1A**) indicates that the TRG and AARG are not pristine, which was expected for this graphene-PMMA composite ink. Furthermore, the subtle shifts in wavenumber peak for the Raman bands (relative to pristine single layer graphene) are likely due to: 1) the presence of aggregated graphene islands (see also **Fig 2** and related discussion), 2) surface bound PMMA within the composite, and 3) use of a 532 nm monochromatic laser, or 4) residual solvent effects after washing. Chemical reduction with ascorbic acid (i.e., AARG) also caused a slight bathochromic shift (approximately 10 cm^{-1}) in the D-band (**Fig 1A**) and the G-band (**Fig 1B**), which is most like due to residual solvent effects.

The intensity of the D-, G-, and 2D-bands for AARG were significantly lower than TRG ($p=0.01$; $\alpha=0.05$; see supplemental **Fig S2**), which is similar to studies of pristine graphene (Stankovich et al., 2007). Furthermore, the intensity ratio (I_D/I_G) for AARG (0.79 ± 0.01) was significantly lower than TRG (0.83 ± 0.01), which is indicative of partial removal of hydroxyl groups during reduction of graphene (Tanizawa et al., 2012). The I_D/I_G ratio decreases in the low disorder region because the distance between defects is reduced, as hydroxyl groups contribute to the disorder as apparent in the D band (Childres et al., 2013).

The electron micrographs in **Fig 1 D-F** show distinct changes in surface morphology after each progressive treatment during fabrication of the conductive paper. The TRG ink on nanocellulose paper (**Fig 1D**) contained plate like structures similar to the islands shown by Ramanathan et al (Ramanathan et al., 2008). Gomez-Navarro et al (Gómez-Navarro et al., 2010) and others have shown that composites with reduced graphene oxide (rGO) contain more than 50% of these aggregated reduced graphene

oxide (rGO) islands interspersed with amorphous sp^2 bonded clusters. After ascorbic acid reduction (AARG; **Fig 1E**), the surface area increased, and there were discernable pores in the electron micrograph (approximately 200 nm). Wang et al (Wang et al., 2013) showed that defect clusters in rGO islands can be selectively removed with acid to produce a graphene nanomesh structure with graphene basal planes, enhancing surface area and conductivity. Although we did not explore longer chemical reduction times or stronger acid treatments, (i.e., larger pores), the 200 nm pores developed here may be related to the enhanced conductivity after chemical reduction based on Wang et al (Wang et al., 2013) (see **Fig 2** for electrochemical data). EDS analysis (see supplemental Table S1) confirmed that the graphene oxide was reduced by thermal/chemical treatment. The carbon-oxygen weight ratio decreased by 11.2%, and the atomic carbon-oxygen ratio decreased by 9.7% after chemical treatment with ascorbic acid. **Fig 1F** shows platinum nano cauliflower structures that were formed on the rGO-CNC paper after chemical reduction of graphene oxide. Platinum nanocauliflowers with structures ranging from 10 nm nodes to 2 μm terminal clusters were homogenously distributed across the surface. The specific particle size, or fractal dimension, of these platinum nanostructures was not determined. As noted by Kim et al (Kim, 2004), three dimensional fractal structures are inherently difficult to quantify for cauliflower structures. After formation of nanocauliflowers, the oxygen was reduced by 88%, and surface coverage of graphene was reduced by 97% (see supplemental Table S1 and Fig S3). EDS spectra also confirmed the presence of two types of platinum (PtM and PtLα), which is similar to previous work with rGO-nPt nanostructures (Chaturvedi et al., 2014). The detection of a relatively small PtLα peak (edge energy = 3.3 keV) relative

to the Pt_M peak (edge energy = 9.4 keV) indicates that the platinum structure is stable up to the penetration depth of the X ray (approximately 1-2 μm). No peaks for Pt oxide were observed, although Taguchi et al (Taguchi et al., 2016) recently showed formation of Pt oxide using similar metal deposition techniques on commercial Pt/Ir electrodes.

No cracks or structural abnormalities were observed in the nanoplatinum (also see supplemental Fig S3), and no capping agents or quaternary ammonium salts were used to form the fractal nanometal structures.

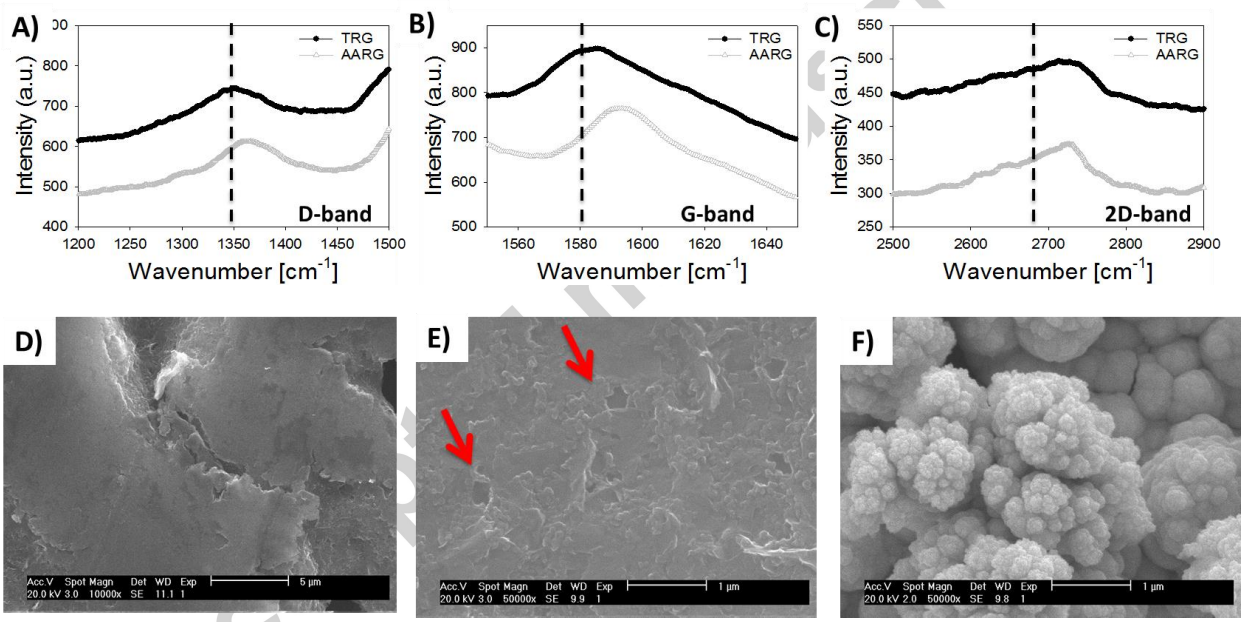

Figure 1. Panels A-C: Raman spectrographs of TRG and AARG using a 532 nm laser excitation showing **A)** D-band, **B)** G-band, and **C)** 2D-band. Stokes shifts after partial reduction of graphene oxide are shown in the G-band and 2D bands, while Anti-stokes shift are shown for the D-band. Full Raman spectra are shown in supplemental Figure S2. Panels D-F: SEM images of conductive paper surface following each treatment. (D) TRG ink on cellulose paper with irregular reduced graphene oxide microplatelet

structures, (E) AARG with heterogeneous 200 nm pores (indicated by arrows), and (F) pulSED nano cauliflowers on the reduced graphene oxide ink.

Although a deterministic electron transport model has yet to be developed, a number of researchers have empirically demonstrated that nanometal cauliflower, broccoli, and raspberry structures have extremely high electron transport relative to other nanometal morphologies. Simonet (Simonet, 2006) demonstrated the formation of Pt nano raspberry structures using galvanostatic electrodeposition in the presence of dimethylformamide and tetraalkylammonium salts. Other non-fractal nanoscale platinum morphologies used in electrochemical biosensing include micro-islands (McLamore et al., 2011; Shi et al., 2011), nanosphere-decorated carbon nanotubes (Claussen et al., 2012, 2011, 2009), graphene-nanocoral sandwich films (Chaturvedi et al., 2014; Vanegas et al., 2014), and multi-layered graphene-nanosphere petals (Claussen et al., 2011). The recent interest in fractal nanostructures for electronic applications is in essence a form of biomimicry; natural systems have evolved fractal patterns that optimize mass transfer, heat transfer, and structural integrity utilizing a vast array of fractal morphologies (Kane et al., 1999; Sawada et al., 1986; Sims et al., 2008).

3.2 Electrochemical Analysis

Thermal reduction of the graphene-nanocellulose paper did not produce well-defined CV peaks using either ferrocyanide or with the ferrocyanide/ferricyanide redox couple (**Fig 2A**). This indicates that the TRG paper had poor charge transfer (also see supplemental Figure S4). Chemical reduction of the graphene ink increased the peak

current response, but the change in redox peak was not significant ($p=0.31$; $\alpha=0.05$). When platinum nanocauliflowers were deposited on the AARG graphene, well-defined reversible redox peaks were apparanet, and the peak current increased by 160 ± 12 μA (**Fig 2A**). Representative Nyquist plots (**Fig 2B**) and Bode magnitude plots (**Fig 2C**) confirm this trend; TRG and AARG had a relatively high charge transfer resistance (Rct) at low frequency impedance values (indicated by the semicircular region), and diffusion limitations at high frequency. However, EIS for the Pt nano cauliflower-decorated AARG paper did not have an obvious semicircular region, which indicates the charge transfer resistance was negligible (also see **Fig 3** and Table 1). For all samples, the solution resistance did not change significantly (see supplemental Figure S5 for solution resistance data and the Randles-Ershler equivalent circuit model). The Bode magnitude plots in **Fig 2C** indicate that charge transfer in the TRG and AARG conductive paper was diffusion limited, but not in the Pt nanocauliflower-decorated samples (also see supplemental Figure S6).

247

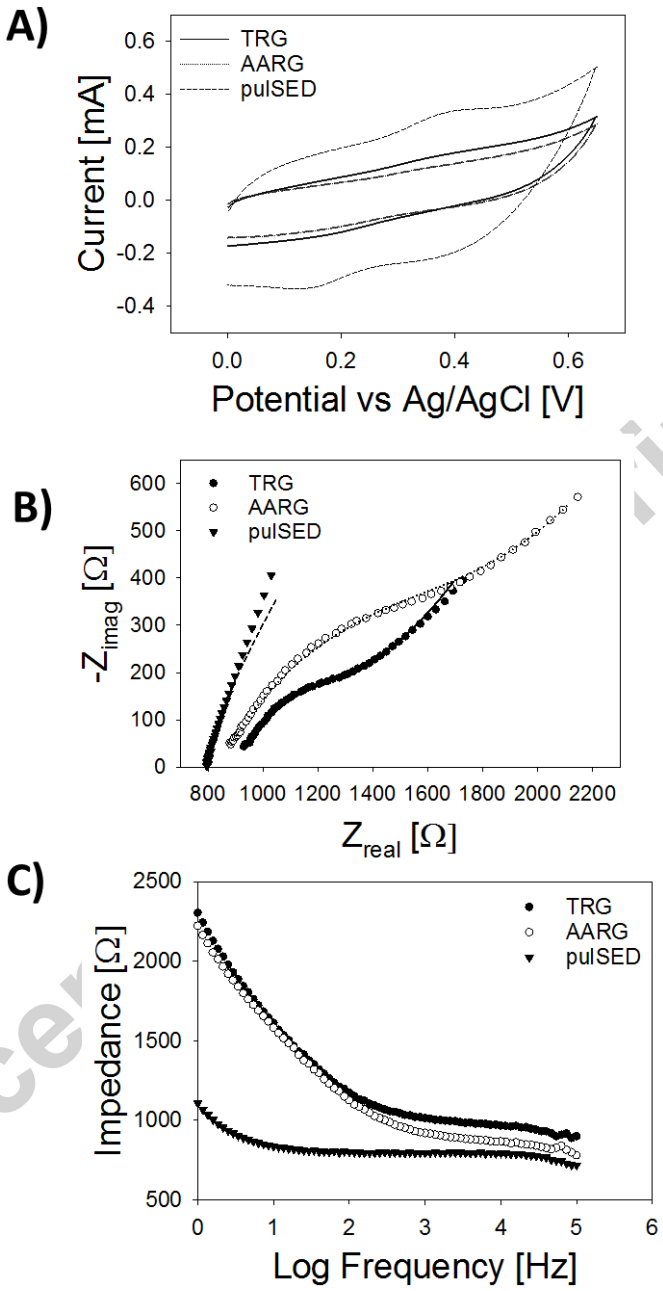

248
249 **Figure 2**. Electrochemical behavior of graphene-nanocellulose conductive paper for
250 each treatment. Representative **A)** cyclic voltammograms at a scan rate of 100 mV/sec
251 and switching potential of 650 mV, **B)** Bode magnitude plot, and **C)** Bode phase plot.
252
253

Fig 3 shows the average CV and EIS data for each material (n>3). The average electroactive surface area (ESA) increased by an order of magnitude after deposition of Pt nanocauliflower structures (**Fig 3A**). For the data in **Fig 3A,** only the nano Pt-decorated material showed well-defined, reversible redox peaks that can be used for calculation of ESA using Randles-Sevcik. On the other hand, the AARG and TRG samples produced "bird beak" shaped voltammograms similar to nanoelectrodes, with no distinct oxidation or reduction peak (supplemental Fig S4); thus we estimate peak reductive current as an approximation only for comparison purposes to calculate average ESA for the three nanomaterials as shown in **Fig 3A**. Although there is significant variation in the ESA for all materials, the deposition of pulSED Pt nanocauliflowers on AARG-CNC paper significantly improved ESA to an average value of 0.29 ± 0.13 cm^2 (see **Table 1** for a comparison to other devices in the published literature),

The average R_{ct} of Pt nano cauliflower ($24 \pm 6\ \Omega$) was was orders of magnitude lower than R_{ct} for TRG ($980 \pm 162\ \Omega$) and AARG ($1720 \pm 206\ \Omega$) paper (ANOVA, $p=0.010$, $\alpha=0.05$) (**Fig 3B**). The average Warburg resistance for the TRG ($1.7 \pm 0.1\ k\Omega$) and AARG ($1.9 \pm 0.2\ k\Omega$) was significantly higher than the Pt nano cauliflower decorated graphene ($1.1 \pm 0.1\ k\Omega$) (see **Fig 3B**). This result, and the Bode phase plots in supplemental Figure S6, indicate that diffusive transport limitations reduce the sensing performance of TRG and AARG conductive paper, but performance is enhanced significantly after metallization. Although mixing and increase in operating temperature would likely reduce these effects for TRG and AARG nanocellulose paper,

277 the Pt nano cauliflower device was highly efficient at room temperature and with no
278 solution convection, which is a major advantage for application in POC biosensing.
279 Although capacitance is not a critical parameter for electrochemical biosensing in paper
280 diagnostic devices, **Fig 3B** also shows that the average double layer capacitance for the
281 Pt nano cauliflower graphene paper (1.00 ± 0.02 F) was significantly higher than the
282 TRG (0.52 ± 0.04 F) and the AARG (0.59 ± 0.03 F) graphene paper based on ANOVA
283 ($p < 0.01$; α=0.05).

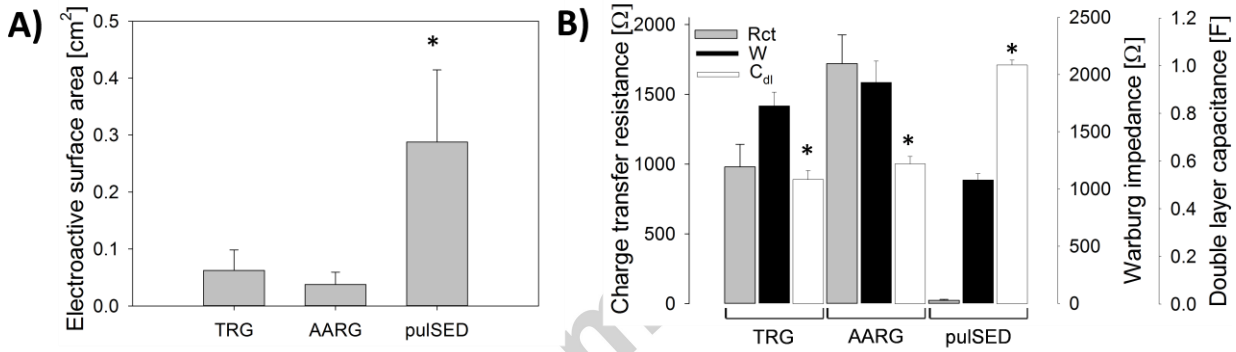

284

285 **Figure 3**. Average electrochemical performance for each treatment of graphene-
286 nanocellulose paper. **A)** Average electroactive surface area. **B)** Average charge transfer
287 resistance (Rct) , Warburg impedance (W), and double layer capacitance (C_{dl}) from a
288 Randles-Ershler equivalent circuit. Error bars represent standard error of the arithmetidc
289 mean. Asterisk (*) indicates significant difference in the arithmetic mean based on
290 Tukey pairwise comparison ($p < 0.05$, $n>3$).

291

292 As shown in **Table 1**, the average ESA for the Pt nanocauliflower-decorated
293 graphene paper (0.29 ± 0.05 cm^2) is within the same range as previously reported
294 nanocarbon/nanoplatinum devices used based on commercial electrodes and silicon
295 biochips. The ESA of the nanocauliflower AARG paper was similar to platinum

nanosphere sandwich structures formed on reduced graphene oxide (rGO) using a commercial Pt/Ir electrode (Vanegas et al., 2014) and amorphous nanoplatinum formed on nanoceria-functionalized rGO electrodes (Chaturvedi et al., 2014) when normalized for electrode diameter. The ESA was higher than platinum microstructures formed on carbon nanotube-modified Pt/Ir electrodes (McLamore et al., 2011; Shi et al., 2011) or carbon-ceramic electrodes (Habibi and Razmi, 2012). Surprisingly, the paper based electrode exhibits approximately five times higher ESA than low-density SWCNT arrays grown from the pores of porous anodic alumina and decorated with platinum carbon nanotubes (Claussen et al., 2011) when accounting for electrode surface area. Therefore the Pt nanocauliflower-decorated graphene paper displays a potential low-cost route to create highly electroactive, carbon/Pt nanostructured electrodes as opposed to higher cost fabrication routes that use chemical vapor deposition and photolithography patterning. This is not a head-to-head comparison of the graphene paper in this manuscript to similar silicon based biochips devices since the density of nanostructures is not the same. However, the comparison highlights the excellent potential for this low cost and simple material as a biosensing platform. A brief shelf life study indicated that the Pt nanocauliflower-decorated paper maintained 90% of the reported electroactive surface area when stored in a desiccator at room temperature for at least 30 days, but completely deteriorated after 30 days; the paper was extremely brittle and testing of ESA was not possible using the methods herein after 30 days so no data can be shown (see supplemental Figure S7 for photos of paper).

Table 1. Performance characteristics for various nanocarbon-nanometal hybrid composite transducer layers for electrochemical biosensing

Type of sensor	Platform	Electroactive surface area (cm^2 $X10^{-2}$)	Physical surface area [cm^2]	Reference
Nanocellulose paper	TRG paper	0.06 ± 0.01	0.03	*This work*
	AARG paper	0.04 ± 0.02	0.03	*This work*
	Pt nanocauliflowers/ AARG paper	0.29 ± 0.05	0.03	*This work*
Pt/Ir electrode	Pt nanocoral/ MWCNT sandwich	0.07 ± NR	0.02	(Vanegas et al., 2014)
	Pt nanocoral/ graphene sandwich	0.18 ± NR	0.02	(Vanegas et al., 2014)
	Amorphous Pt/nCe/graphene	0.05 ± 0.02	0.02	(Chaturvedi et al., 2014)
	Pt black/graphene	0.6 ± 0.10	0.02	(Shi et al., 2011)
	Pt microislands/ MWCNT/TMOS	0.7 ± NR	0.02	(McLamore et al., 2011)
Carbon-ceramic electrode	AgNP/ SWCNT	0.3 ± NR	0.22	(Habibi and Razmi, 2012)
Silicon biochip	Pt nanosphere/ SWCNT	0.02 ± 0.005	0.50	(Claussen et al., 2011)

MWCNT = multiwalled carbon nanotube
SWCNT = single walled carbon nanotube
nCe = nanoceria
AgNP = silver nanoparticle
TMOS = tetramethyl orthosilicate sol gel

In the next section, the nanoplatinum decorated graphene paper was used to develop an amperometric glucose biosensor and a RNA aptasensor for detecting *E. coli* O157:H7 as a proof of concept using the approach described by McLamore et al (2011) and Chaturvedi et al (2014) (see supplemental Figure S8 for a schematic of the working principle of each device).

331

332 *3.3 Amperometric biosensing*

333 Prior to testing for glucose, each treatment of the graphene-nanocellulose paper
334 was tested for sensitivity, LOD and response time towards hydrogen peroxide using
335 DCPA at + 500 mV (see supplemental Figure S9 for details). The average sensitivity
336 (2.9 ± 0.4 mA mM^{-1}), LOD (0.2 ± 0.1 µM), and response time (6.5 ± 0.5 sec) are shown
337 in **Fig 4A**; all values were within the range of laboratory electrodes and biochips
338 functionalized with graphene-nanometal hybrid materials for detection of peroxide
339 (Chaturvedi et al., 2014; Claussen et al., 2011; Vanegas et al., 2014). Although
340 hydrogen peroxide detection was not a major focus of this work, these results
341 demonstrate that the paper based nanomaterial device has many potential applications
342 for sensing and biosensing, and is capable of competing with conventional laboratory
343 probes. The average sensitivity, limit of detection (LOD) and response time for
344 enzymatic glucose biosensors prepared on the graphene nanocellulose paper was also
345 tested using DCPA. A representative time-series plot of oxidative current for a Pt
346 nanocauliflower decorated graphene paper device after stepwise addition of 50 µM
347 glucose is shown in **Fig 4A** (arrows indicate addition of glucose). The average
348 sensitivity for replicate biosensors (n=3) is shown in **Fig 4B;** average sensitivity was
349 3.59 ± 0.68 mA mM^{-1}, which is lower or within the range of laboratory electrochemical
350 devices fabricated on glass, silicon, Katpon tape, and other materials. The average LOD
351 (0.08 ± 0.02 µM), and response time (8.8 ± 1.8 sec) toward glucose are applicable for
352 POC testing of glucose levels in saliva, tears, or diluted blood (approximately 10X

353 dilution). The response time toward glucose changed significantly within the testing

354 range, but was less than 10 sec, and as low as 6 sec.

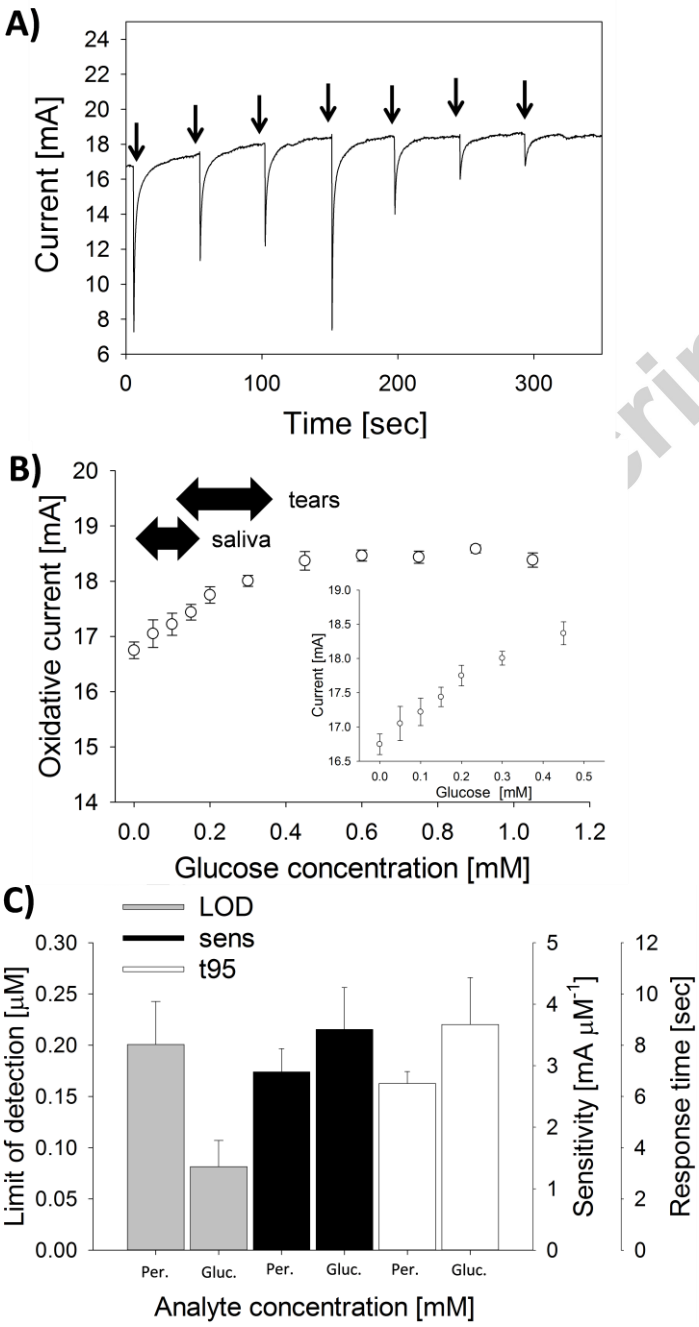

355

356 **Figure 4**. Glucose biosensor developed using the graphene-nanocellulose paper. DC

357 potential amperometry was used to calculate the sensitivity, limit of detection (LOD) and

358 response time (t_{95}) **A)** Representative oxidative current response to injections of 50 µM

359 glucose (indicated by vertical arrows). **B)** Average calibration curves for glucose derived
360 from replicate DCPA tests (n=3). Inset shows linear range between 0 to 500 µM. **C)**
361 Average LOD, sensitivity, and t_{95} for peroxide and glucose biosensors tested in buffer
362 at 25 °C; Per.=hydrogen peroxide data, Gluc.= Glucose data. Error bars represent the
363 standard error of the mean.
364
365 *3.4 Bacteria detection*
366 As a second demonstration of the versatile material, an aptasensor was
367 developed for measuring *E. coli* O157:H7 (see supplemental Figure S8 for a schematic
368 of the working principle). **Fig. 5** shows a representative Nyquist plot (**Fig 5a**) and Bode
369 plot (**Fig 5b**). Calibration curves obtained from the charge transfer resistance (derived
370 using a Randles equivalent circuit) and the impedance at 1 Hz (from Bode plot) are
371 shown in **Fig 5c-d**. The calibration plots for both measurements (**Fig 5c**) follow a non-
372 linear saturation behavior, and the rate constant for each plot is nearly identical (≈ 0.01
373 mL CFU^{-1}), as expected. The analysis frequency of 1 Hz was selected from Bode plots
374 considering the total change in measured impedance (ΔZ') and the rate constant
375 associated with the non-linear calibration plot (see **Fig S10** for details of the frequency
376 optimization). As expected, log frequency plots indicated no change in impedance at
377 high frequency, indicative of the solution resistance. The average sensitivity from each
378 plot derived from the impedance value at 1Hz (**Fig 5d**) was 16.1 Ω/log CFU mL^{-1} for the
379 direct impedance measurement (Z'**=** 16.1*log CFU mL^{-1} + 4699 Ω (R^2=0.85)), and 20.1
380 Ω/log CFU mL^{-1} from the charge transfer resistance (R_{ct} = 20.1*log CFU mL^{-1} + 1937Ω
381 (R^2=0.97)) derived from the Randles circuit. Based on these two plots, the LOD was 3.5

± 1.1 CFU mL^{-1} for the impedance plot and 4.2 ± 0.8 for the charge transfer resistance (S/N ratio = 3). A brief kinetic study indicated that aptamer-*E. coli* binding is positively cooperative (i.e., there is interaction between binding sites). The Hill coefficient was greater than 1.0 using both Scratchard and Klotz theorems, which indicates cooperative binding (see **Fig. S11)**.

For both measurements, the signal at 1 CFU mL^{-1} was significantly higher than baseline ($p<0.001$, $\alpha=0.05$), although calculation of LOD using the 3δ method indicated that the minimum detectable value in vegetable broth may be closer to ≈4 CFU mL^{-1}. Using the calculated LOD above, the linear range using both Z' and R_{ct} as the output was from 4 to 10^5 CFU/mL with an average response time of 12 min (including 10 min for bacteria capture and 2 min for EIS). This LOD is relevant for food safety and public health since the infectious dose for *E. coli* O157:H7, which is estimated to be 10 to 100 cells. The shiga toxin-producing serotype is implicated in the most incidents of illness worldwide (USFDA, 2015). These infections are mostly food and water borne and have implicated undercooked chicken and ground beef, raw milk, cold sandwiches, water, unpasteurized apple juice, and sprouts and vegetables.

The performance values obtained in this study (LOD, response time and sensitivity) are comparable to, if not superior to, aptasensors published for the detection of *E. coli* O157:H7. Most recently, Ning et al. (Ning et al., 2015) developed an impedance-based immunosensor for O157:H7 based on self-assembled lectins with a LOD of 100 CFU mL^{-1}, a linear range from 10^2 to 10^7 CFU mL^{-1}, and a total detection time of 1 h. Fang et al. (Fang et al., 2014) developed a lateral flow biosensor based on aptamer-mediated strand displacement amplification with a detection limit of 10 CFU

405 mL^{-1}; however, it required pre-enrichment steps and isothermal amplification prior to

406 lateral flow test.

407

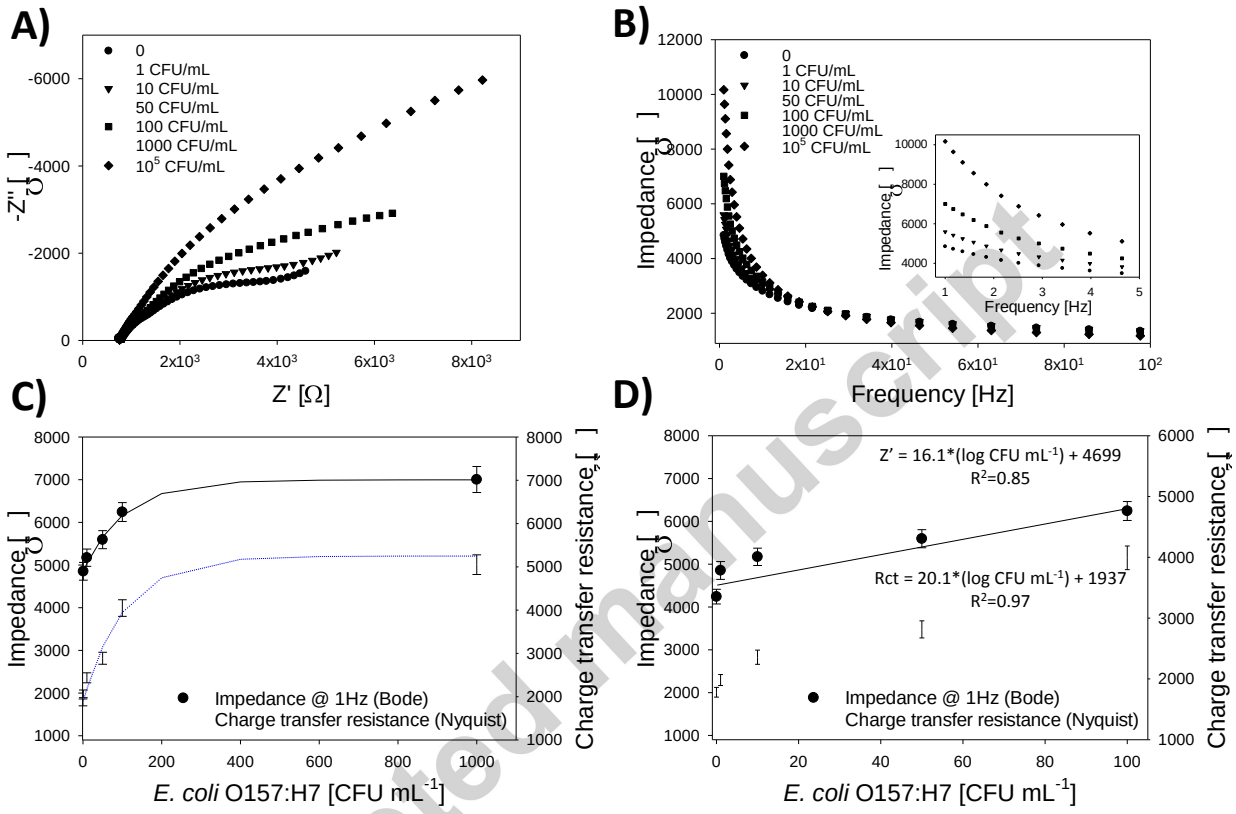

408

409 **Figure 5**. Representative **A)** Nyquist and **B)** Bode magnitude plot (inset shows

410 exploded view of lower frequency range) **C)** Calibration curve using direct impedance

411 measurement and charge transfer resistance (n=3). **D)** Exploded view of linear sensing

412 region from panel C.

413

414 We have demonstrated the first reported development of graphene paper

415 decorated with platinum nanocauliflower for use in electrochemical biosensing of small

416 molecules (glucose) or detection of pathogenic bacteria (*Escherichia coli* O157:H7). The

417 highly sensitive paper biosensor platform is low cost (less than $4 per sample; with

most of the cost derived from the platinum), lightweight, rapid, and reproducible by any biosensing laboratory. The device has a number of potential applications in point of care biosensing, particularly in developing regions where access to conventional fabrication equipment is not likely. Furthermore, the material could be improved by replacing the platinum with more abundant nanometals such as copper oxide (M et al., 2015; Somturk et al., 2015). This work represents the first example of highly conductive graphene paper that can compete with commercial metal electrodes for biosensing (**Fig 4** and **Fig 5**). For example, Dungchai et al (Dungchai et al., 2009) report one of the first electrochemical biosensors based on paper using a combination of photolithography and screen printing to create 1.3 mm^2 working electrodes on cellulose filter paper for detection of uric acid, glucose, and lactate. Li et al (Li et al., 2014) demonstrated an electrochemical paper biosensor for detection of prostate protein antigen (PSA). The device by Li et al was fabricated by electrochemical synthesis of manganese oxide nanowires on gold nanoparticle “seeds” entrapped in a cellulose matrix. Kong et al (Kong et al., 2014) developed a screen printed electrode for glucose biosensing that used a paper disk, but the paper disk was used to concentrate a blood sample where the recognition/transduction steps were carried out on a paper electrode. In our work, the sample capture, recognition, and transduction steps all occur with one strip of conductive paper in the absence of any exogenous reagents such as ferrocene carboxylic acid. In addition to biosensing, the conductive paper has possible future diverse application in other areas, as demonstrated in development of printed circuit boards (Siegel et al., 2010), bioassays (Kuek Lawrence et al., 2014), 3D cell culture devices (Derda et al., 2011), and energy production/storage (Antolini, 2012).

4. Conclusions

For the first time, we develop fractal nanoplatinum (cauliflower-like) on graphene-nanocellulose paper, and the highly conductive structure is free of any discernable cracks or voids. Material analysis and electrochemical testing, together with the proof of concept testing show that the platinum nano cauliflower-functionalized graphene paper developed here is an extremely efficient material for use in electrochemical biosensing. The paper biosensor showed an extremely low detection limit for glucose (enzymatic biosensor) or *E. coli* O157:H7 (RNA aptasensor), which demonstrates that the facile material can potentially be applied in a diverse array of environmental, agricultural, and medical applications for POC biosensing This important finding shows that the graphene paper developed here is an excellent transducer platform for paper based biosensing and has a range of potential other applications in the area of electronic paper based devices. This represents a significant advance in electrochemical biosensing, as no laborious/expensive equipment, capping agents, or cofactors were used to develop the biosensor.

5. Acknowledgements

The authors would like to thank the National Science Foundation Nanobiosensors program (C. Gomes and E.S. McLamore; Grant No. 1511953-Nanobioensing), the UF Agricultural and Biological Engineering Fellowship (SLB), UF/FAMU Feeder Fellowship (SLB), and the NASA Florida Space Grant Consortium

(EM; grant no. 00091356) for funding. We also thank Brent Gila for support with Raman spectroscopy.

6. References

Abe, K., Suzuki, K., Citterio, D., 2008. Inkjet-printed microfluidic multianalyte chemical sensing paper. Anal. Chem. 80, 6928–6934. doi:10.1021/ac800604v

Antolini, E., 2012. Graphene as a new carbon support for low-temperature fuel cell catalysts. Appl. Catal. B Environ. 123-124, 52–68. doi:10.1016/j.apcatb.2012.04.022

Burrs, S.L., Vanegas, D.C., Bhargava, M., Mechulan, N., Hendershot, P., Yamaguchi, H., Gomes, C., Mclamore, E.S., 2015. A comparative study of graphene–hydrogel hybrid bionanocomposites for biosensing. Analyst 140. doi:10.1039/c4an01788a

Chamousis, R.L., Chang, \Lilian, Watterson, W.J., Montgomery, R.D., Taylor, R.P., Moule, A.J., Shaheen, S.E., Ilan, B., Lagemaatf, J. van de, Osterloh, F.E., 2014. Effect of fractal silver electrodes on charge collection and light distribution in semiconducting organic polymer films. J. Mater. Chem. A 2, 16608–16616.

Chaturvedi, P., Vanegas, D.C., Taguchi, M., Burrs, S.L., Sharma, P., Mclamore, E.S., 2014. A nanoceria–platinum–graphene nanocomposite for electrochemical biosensing. Biosens. Bioelectron. 58, 179–185. doi:10.1016/j.bios.2014.02.021

Chen, H., Müller, M.B., Gilmore, K.J., Wallace, G.G., Li, D., 2008. Mechanically Strong, Electrically Conductive, and Biocompatible Graphene Paper. Adv. Mater. 20, 3557–3561. doi:10.1002/adma.200800757

Childres, I., Jauregui, L., Park, W., Cao, H., Chen, Y., 2013. Raman Spectroscopy of Graphene and Related Materials. New Dev. Phot. Mater. Res. 1–20. doi:10.1016/B978-0-444-53175-9.00016-7

Claussen, J.C., Artiles, M.S., McLamore, E.S., Mohanty, S., Shi, J., Rickus, J.L., Fisher, T.S., Porterfield, D.M., 2011. Electrochemical glutamate biosensing with nanocube and nanosphere augmented single-walled carbon nanotube networks: a comparative study. J. Mater. Chem. 21, 11224. doi:10.1039/c1jm11561h

Claussen, J.C., Franklin, A.D., Haque, A.U., Marshall Porterfield, D., Fisher, T.S., 2009. Electrochemical Biosensor of nanocube-augmented carbon nanotube networks. ACS Nano 3, 37–44. doi:10.1021/nn800682m

Claussen, J.C., Kumar, A., Jaroch, D.B., Khawaja, M.H., Hibbard, A.B., Porterfield, D.M., Fisher, T.S., 2012. Nanostructuring platinum nanoparticles on multilayered graphene petal nanosheets for electrochemical biosensing. Adv. Funct. Mater. 22, 3399–3405. doi:10.1002/adfm.201200551

Derda, R., Tang, S.K.Y., Laromaine, A., Mosadegh, B., Hong, E., Mwangi, M., Mammoto, A., Ingber, D.E., Whitesides, G.M., 2011. Multizone paper platform for 3D cell cultures. PLoS One 6, 1–14. doi:10.1371/journal.pone.0018940

Dikin, D. a, Stankovich, S., Zimney, E.J., Piner, R.D., Dommett, G.H.B., Evmenenko, G., Nguyen, S.T., Ruoff, R.S., 2007. Preparation and characterization of graphene oxide paper. Nature 448, 457–460. doi:10.1038/nature06016

506 Dungchai, W., Chailapakul, O., Henry, C.S., 2009. Electrochemical detection for paper-
507 based microfluidics. Anal. Chem. 81, 5821–5826. doi:10.1021/ac9007573
508 Eda, G., Fanchini, G., Chhowalla, M., 2008. Large-area ultrathin films of reduced
509 graphene oxide as a transparent and flexible electronic material. Nat. Nanotechnol.
510 3, 270–274. doi:10.1038/nnano.2008.83
511 Eda, G., Mattevi, C., Yamaguchi, H., Kim, H., Chhowalla, M., 2009. Insulator to
512 semimetal transition in graphene oxide. J. Phys. Chem. C 113, 15768–15771.
513 doi:10.1021/jp9051402
514 Ellerbee, A.K., Phillips, S.T., Siegel, A.C., Mirica, K. a., Martinez, A.W., Striehl, P., Jain,
515 N., Prentiss, M., Whitesides, G.M., 2009. Quantifying colorimetric assays in paper-
516 based microfluidic devices by measuring the transmission of light through paper.
517 Anal. Chem. 81, 8447–8452. doi:10.1021/ac901307q
518 Fang, Z., Wu, W., Lu, X., Zeng, L., 2014. Lateral flow biosensor for DNA extraction-free
519 detection of Salmonella based on aptamer mediated strand displacement
520 amplification. Biosens. Bioelectron. 56, 192–7. doi:10.1016/j.bios.2014.01.015
521 Ge, J., Lei, J., Zare, R.N., 2012. Protein–inorganic hybrid nanoflowers. Nat.
522 Nanotechnol. 7, 428–432. doi:10.1038/nnano.2012.80
523 Gómez-Navarro, C., Meyer, J.C., Sundaram, R.S., Chuvilin, A., Kurasch, S., Burghard,
524 M., Kern, K., Kaiser, U., 2010. Atomic structure of reduced graphene oxide. Nano
525 Lett. 10, 1144–1148. doi:10.1021/nl9031617
526 Habibi, E., Razmi, H., 2012. Glycerol electrooxidation on Pd, Pt and Au nanoparticles
527 supported on carbon ceramic electrode in alkaline media. Int. J. Hydrogen Energy
528 37, 16800–16809. doi:10.1016/j.ijhydene.2012.08.127
529 Izaki, M., Watanabe, M., Aritomo, H., Yamaguchi, I., Asahina, S., Shinagawa, T.,
530 Chigane, M., Inaba, M., Tasaka, A., 2008. Zinc Oxide Nano-Cauliflower Array with
531 Room Temperature Ultraviolet Light Emission. Cryst. Growth Des. 8, 1418–1421.
532 doi:10.1021/cg070164s
533 Kabiri, S., Tran, D.N.H., Altalhi, T., Losic, D., 2014. Outstanding adsorption performance
534 of graphene-carbon nanotube aerogels for continuous oil removal. Carbon N. Y. 80,
535 523–533. doi:10.1016/j.carbon.2014.08.092
536 Kane, R.S., Takayama, S., Ostuni, E., Ingber, D.E., Whitesides, G.M., 1999. Patterning
537 proteins and cells using soft lithography. Biomaterials 20, 2363–2376.
538 doi:10.1016/S0142-9612(99)00165-9
539 Kim, S.-H., 2004. Fractal structure of a white cauliflower 46, 474–477.
540 Kong, F.Y., Gu, S.X., Li, W.W., Chen, T.T., Xu, Q., Wang, W., 2014. A paper disk
541 equipped with graphene/polyaniline/Au nanoparticles/glucose oxidase
542 biocomposite modified screen-printed electrode: Toward whole blood glucose
543 determination. Biosens. Bioelectron. 56, 77–82. doi:10.1016/j.bios.2013.12.067
544 Kuek Lawrence, C.S., Tan, S.N., Floresca, C.Z., 2014. A “green” cellulose paper based
545 glucose amperometric biosensor. Sensors Actuators, B Chem. 193, 536–541.
546 doi:10.1016/j.snb.2013.11.054
547 Labroo, P., Cui, Y., 2014. Graphene nano-ink biosensor arrays on a microfluidic paper
548 for multiplexed detection of metabolites. Anal Chim Acta 813, 90–96.
549 doi:10.1016/j.aca.2014.01.024
550 Li, L., Xu, J., Zheng, X., Ma, C., Song, X., Ge, S., Yu, J., Yan, M., 2014. Growth of gold-
551 manganese oxide nanostructures on a 3D origami device for glucose-oxidase label

based electrochemical immunosensor. Biosens. Bioelectron. 61, 76–82. doi:10.1016/j.bios.2014.05.012

Liu, C., Su, F., Liang, J., Huang, P., 2014. Facile fabrication of superhydrophobic cerium coating with micro-nano flower-like structure and excellent corrosion resistance. Surf. Coatings Technol. 258, 580–586. doi:10.1016/j.surfcoat.2014.08.032

Liu, H., Crooks, R.M., 2011. Three-dimensional paper microfluidic devices assembled using the principles of origami. J. Am. Chem. Soc. 133, 17564–17566. doi:10.1021/ja2071779

Liu, J., 1998. Fullerene Pipes. Science (80-.). 280, 1253–1256. doi:10.1126/science.280.5367.1253

M, B.S., Hancer, M., Ocsoy, I., Özdemir, N., 2015. No TitleSynthesis of copper ion incorporated horseradish peroxidase-based hybrid nanoflowers for enhanced catalytic activity and stability. Dalt. Trans. 44, 13845–13852.

Madden, J.D.W., Barisci, J.N., Anquetil, P. a., Spinks, G.M., Wallace, G.G., Baughman, R.H., Hunter, I.W., 2006. Fast carbon nanotube charging and actuation. Adv. Mater. 18, 870–873. doi:10.1002/adma.200502136

Marr, K.M., Chen, B., Mootz, E.J., Geder, J., Pruessner, M., Melde, B.J., Vanfleet, R.R., Medintz, I.L., Iverson, B.D., Claussen, J.C., 2015. High Aspect Ratio Carbon Nanotube Membranes Decorated with Pt Nanoparticle Urchins for Micro Underwater Vehicle Propulsion via H 2 O 2 Decomposition 9, 7791–7803. doi:10.1021/acsnano.5b02124

Mates, J.E., Bayer, I.S., Salerno, M., Carroll, P.J., Jiang, Z., Liu, L., Megaridis, C.M., 2015. Durable and flexible graphene composites based on artists' paint for conductive paper applications. Carbon N. Y. 87, 163–174. doi:10.1016/j.carbon.2015.01.056

McLamore, E.S., Shi, J., Jaroch, D., Claussen, J.C., Uchida, a, Jiang, Y., Zhang, W., Donkin, S.S., Banks, M.K., Buhman, K.K., Teegarden, D., Rickus, J.L., Porterfield, D.M., 2011. A self referencing platinum nanoparticle decorated enzyme-based microbiosensor for real time measurement of physiological glucose transport. Biosens. Bioelectron. 26, 2237–45. doi:10.1016/j.bios.2010.09.041

Ning, Y., Li, W., Duan, Y., Yang, M., 2015. High Specific DNAzyme-Aptamer Sensor for Salmonella paratyphi A Using Single-Walled Nanotubes – Based Dual Fluorescence-Spectrophotometric Methods. doi:10.1177/1087057114528538

Park, S., Lee, K.-S., Bozoklu, G., Cai, W., Nguyen, S.T., Ruoff, R.S., 2008. Graphene oxide papers modified by divalent ions-enhancing mechanical properties via chemical cross-linking. ACS Nano 2, 572–578. doi:10.1021/nn700349a

Ramanathan, T., Abdala, a a, Stankovich, S., Dikin, D. a, Herrera-Alonso, M., Piner, R.D., Adamson, D.H., Schniepp, H.C., Chen, X., Ruoff, R.S., Nguyen, S.T., Aksay, I. a, Prud'Homme, R.K., Brinson, L.C., 2008. Functionalized graphene sheets for polymer nanocomposites. Nat. Nanotechnol. 3, 327–331. doi:10.1038/nnano.2008.96

Sattayasamitsathit, S., Gu, Y., Kaufmann, K., Minteer, S., Polsky, R., Wang, J., 2013. Tunable hierarchical macro/mesoporous gold microwires fabricated by dual-templating and dealloying processes. Nanoscale 5, 7849–54. doi:10.1039/c3nr02940a

Sawada, Y., Dougherty, A., Gollub, J.P., 1986. Dendritic and Fractal Patterns in

598 Electrolytic Metal Deposits. Phys. Rev. Lett. 56, 1260.
599 doi:10.1103/PhysRevLett.56.1260
600 Shi, J., Claussen, J.C., Mclamore, E.S., Ul Haque, A., Jaroch, D., Diggs, A.R., Calvo-
601 Marzal, P., Rickus, J.L., Porterfield, D.M., 2011. A comparative study of enzyme
602 immobilization strategies for multi-walled carbon nanotube glucose biosensors.
603 Nanotechnology 22. doi:10.1088/0957-4484/22/35/355502
604 Siegel, A.C., Phillips, S.T., Dickey, M.D., Lu, N., Suo, Z., Whitesides, G.M., 2010.
605 Foldable printed circuit boards on paper substrates. Adv. Funct. Mater. 20, 28–35.
606 doi:10.1002/adfm.200901363
607 Simonet, J., 2006. The platinized platinum interface in super-dry solvents: Cathodic
608 reversible reactivity and morphology modifications in the presence of
609 tetramethylammonium salts. J. Electroanal. Chem. 593, 3–14.
610 doi:10.1016/j.jelechem.2006.01.019
611 Sims, D.W., Southall, E.J., Humphries, N.E., Hays, G.C., Bradshaw, C.J. a, Pitchford,
612 J.W., James, A., Ahmed, M.Z., Brierley, A.S., Hindell, M. a, Morritt, D., Musyl, M.K.,
613 Righton, D., Shepard, E.L.C., Wearmouth, V.J., Wilson, R.P., Witt, M.J., Metcalfe,
614 J.D., 2008. Scaling laws of marine predator search behaviour. Nature 451, 1098–
615 1102. doi:10.1038/nature06518
616 Somturk, B., Hancer, M., Ocsoy, I., Özdemir, N., 2015. Synthesis of copper ion
617 incorporated horseradish peroxidase-based hybrid nanoflowers for enhanced
618 catalytic activity and stability. Dalt. Trans. 44, 13845–13852.
619 Spinks, G.M., Wallace, G.G., Fifield, L.S., Dalton, L.R., Mazzoldi, A., De Rossi, D.,
620 Khayrullin, I.I., Baughman, R.H., 2002. Pneumatic carbon nanotube actuators. Adv.
621 Mater. 14, 1728–1732. doi:10.1002/1521-4095(20021203)14:23<1728::AID-
622 ADMA1728>3.0.CO;2-8
623 Stankovich, S., Dikin, D.A., Piner, R.D., Kohlhaas, K.A., Kleinhammes, A., Jia, Y., Wu,
624 Y., Nguyen, S.T., Ruoff, R.S., 2007. Synthesis of graphene-based nanosheets via
625 chemical reduction of exfoliated graphite oxide. Carbon N. Y. 45, 1558–1565.
626 doi:10.1016/j.carbon.2007.02.034
627 Suaifan, G. a R.Y., Esseghaier, C., Ng, A., Zourob, M., 2013. Ultra-rapid colorimetric
628 assay for protease detection using magnetic nanoparticle-based biosensors.
629 Analyst 138, 3735–9. doi:10.1039/c3an36881e
630 Taguchi, M., Schwalb, N., Rong, Y., Vanegas, D.C., Garland, N., Tan, M., Yamaguchi,
631 H., Claussen, J.C., McLamore, E.S., 2016. pulSED: Pulsed sonoelectrodeposition
632 of fractal nanoplatinum for enhancing amperometric biosensor performance.
633 Analyst. doi:10.1039/C6AN00069J
634 Tanizawa, Y., Okamoto, Y., Tsuzuki, K., Nagao, Y., Yoshida, N., Tero, R., Iwasa, S.,
635 Hiraishi, a, Suda, Y., Takikawa, H., Numano, R., Okada, H., Ishikawa, R., Sandhu,
636 a, 2012. Microorganism mediated synthesis of reduced graphene oxide films. J.
637 Phys. Conf. Ser. 352, 012011. doi:10.1088/1742-6596/352/1/012011
638 Ujihara, M., Imae, T., 2013. Versatile one-pot synthesis of confeito-like Au nanoparticles
639 and their surface-enhanced Raman scattering effect. Colloids Surfaces A
640 Physicochem. Eng. Asp. 436, 380–385. doi:10.1016/j.colsurfa.2013.07.003
641 USFDA, 2015. U.S. Food and Drug Administration. Bacteriological Analytical Manual
642 (BAM).
643 http//www.fda.gov/food/foodscienceresearch/laboratorymethods/ucm2006949.htm.

644 2015 [cited 3/10/2016].
645 Vanegas, D.C., Taguchi, M., Chaturvedi, P., Burrs, S., Tan, M., Yamaguchi, H.,
646 Mclamore, E.S., 2014. A comparative study of carbon–platinum hybrid
647 nanostructure architecture for amperometric biosensing. Analyst 139, 660–667.
648 doi:10.1039/c3an01718d
649 Wang, J., Yuan, R., Chai, Y., Li, W., Fu, P., Min, L., 2010. Using flowerlike polymer-
650 copper nanostructure composite and novel organic-inorganic hybrid material to
651 construct an amperometric biosensor for hydrogen peroxide. Colloids Surf. B.
652 Biointerfaces 75, 425–31. doi:10.1016/j.colsurfb.2009.09.015
653 Wang, X., Jiao, L., Sheng, K., Li, C., Dai, L., Shi, G., 2013. Solution-processable
654 graphene nanomeshes with controlled pore structures. Sci. Rep. 3, 1996.
655 doi:10.1038/srep01996
656 Warren, S.C., Voïtchovsky, K., Dotan, H., Leroy, C.M., Cornuz, M., Stellacci, F., Hébert,
657 C., Rothschild, A., Grätzel, M., 2013. Identifying champion nanostructures for solar
658 water-splitting. Nat. Mater. 12, 842–9. doi:10.1038/nmat3684
659 Wei, L., Fan, Y.J., Wang, H.H., Tian, N., Zhou, Z.Y., Sun, S.G., 2012. Electrochemically
660 shape-controlled synthesis in deep eutectic solvents of Pt nanoflowers with
661 enhanced activity for ethanol oxidation. Electrochim. Acta 76, 468–474.
662 doi:10.1016/j.electacta.2012.05.063
663 Wilson, K.C., Manikandan, E., Basheer Ahamed, M., Mwakikunga, B.W., 2014.
664 Nanocauliflower like structure of CdS thin film for solar cell photovoltaic
665 applications: In situ tin doping by chemical bath deposition technique. J. Alloys
666 Compd. 585, 555–560. doi:10.1016/j.jallcom.2013.09.185
667 Xia, F., Perebeinos, V., Lin, Y., Wu, Y., Avouris, P., 2011. The origins and limits of
668 metal-graphene junction resistance. Nat. Nanotechnol. 6, 179–184.
669 doi:10.1038/nnano.2011.6
670 Xu, Y., Sheng, K., Li, C., Shi, G., 2010. Self-assembled graphene hydrogel via a one-
671 step hydrothermal process. ACS Nano 4, 4324–4330. doi:10.1021/nn101187z
672 Yang, G., Lee, C., Kim, J., Ren, F., Pearton, S.J., 2013. Flexible graphene-based
673 chemical sensors on paper substrates. Phys. Chem. Chem. Phys. 15, 1798–801.
674 doi:10.1039/c2cp43717a
675 Zhang, X., Sreekumar, T. V, Liu, T., Kumar, S., 2004. Properties and Structure of Nitric
676 Acid Oxidized Single Wall Carbon Nanotube Films. J. Phys. Chem. B 108, 16435–
677 16440. doi:10.1021/jp0475988
678 Zhang, Z., Ma, M., Chen, C., Caia, Z., Huang, X., 2016. The morphology, structure and
679 electrocatalytic ability of graphene prepared with different drying methodse. RSC
680 Adv. 6, 28005–28014.
681 Zhou, P., Dai, Z., Fang, M., Huang, X., Bao, J., Gong, J., 2007. Novel Dendritic
682 Palladium Nanostructure and Its Application in Biosensing. J. Phys. Chem. C 111,
683 12609–12616. doi:10.1021/jp072898l
684
685

686

687

688

689 Graphical abstract

690

Highlight image. Conductive paper was prepared by decorating graphene-nanocellulose strips with platinum nano cauliflowers. The surface was functionalized with biomaterials (oxidase or RNA) for demonstration as a point of care biosensor.

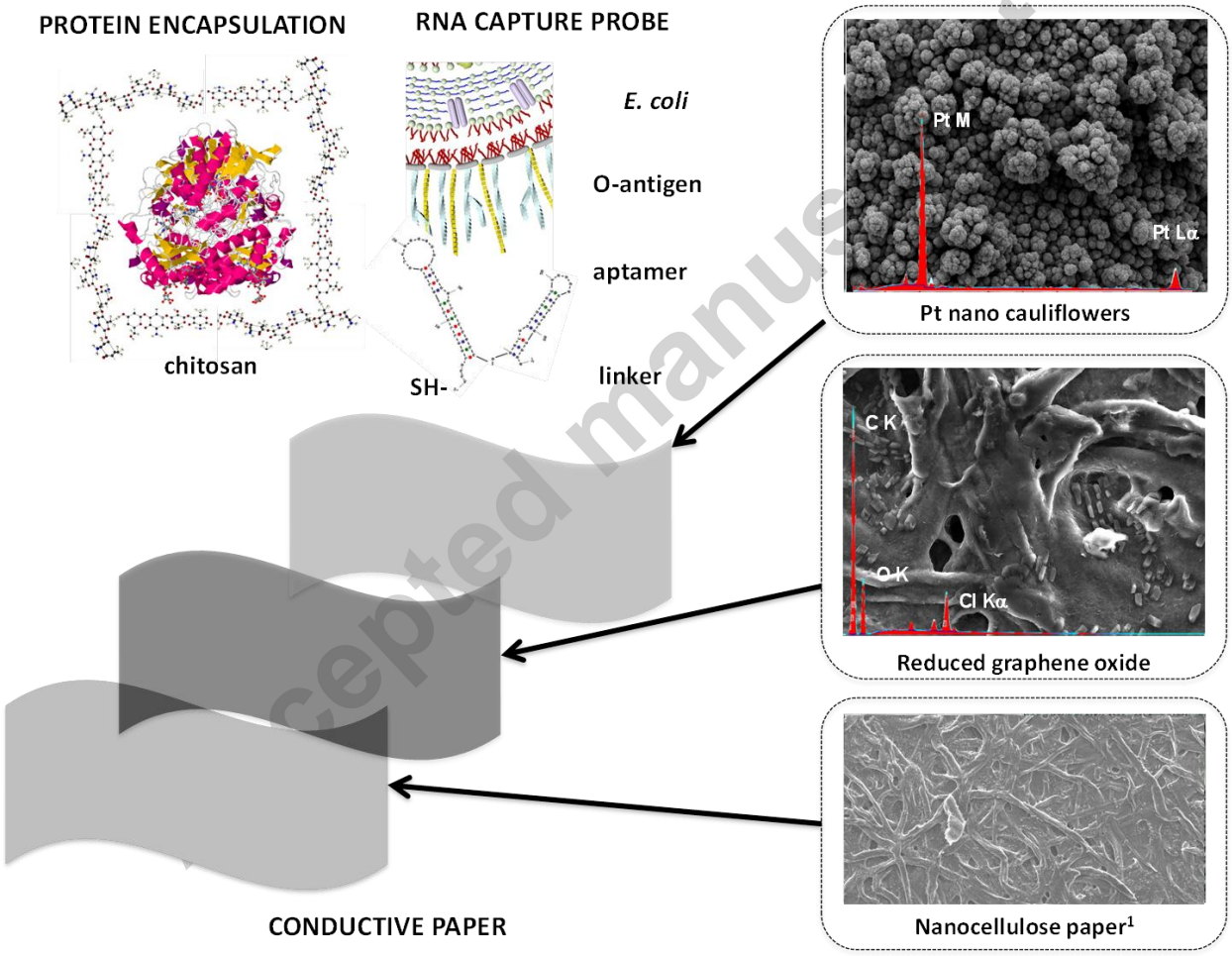

691